

Charmonium-Nucleon Dissociation Cross Sections in the Quark Model

J.P. Hilbert,¹ N. Black,² T. Barnes,^{3,4} and E.S. Swanson¹

¹*Department of Physics and Astronomy, University of Pittsburgh, Pittsburgh PA 15260*

²*Utah Center for Advanced Imaging Research, University of Utah, Salt Lake City, UT 84108*

³*Physics Division, Oak Ridge National Laboratory, Oak Ridge, TN 37831*

⁴*Department of Physics and Astronomy, University of Tennessee, Knoxville, TN 37996*

Charmonium dissociation cross sections due to flavor-exchange charmonium-baryon scattering are computed in the constituent quark model. We present results for inelastic $J/\psi N$ and $\eta_c N$ scattering amplitudes and cross sections into 46 final channels, including final states composed of various combinations of D , D^* , Σ_c , and Λ_c . These results are relevant to experimental searches for the deconfined phase of quark matter, and may be useful in identifying the contribution of initial $c\bar{c}$ production to the open-charm final states observed at RHIC through the characteristic flavor ratios of certain channels. These results are also of interest to possible charmonium-nucleon bound states.

I. INTRODUCTION

The production of heavy quarkonium in heavy ion collisions has long been considered a possible diagnostic for the appearance of exotic QCD phases in relativistic heavy ion collisions [1, 2]. In particular it has been anticipated that the charmonium production cross section in central AA reactions will be suppressed if a quark gluon plasma (QGP) is formed, since the long-range $c\bar{c}$ confining potential will be screened within the QGP. However, this diagnostic can be confounded by subsequent charmonium dissociation due to inelastic hadron rescattering “comover absorption”, which also contributes to the depletion of initially produced charmonium. Alternatively, charmonium can be regenerated due to rescattering of open-charm hadrons in the late stages of heavy ion collisions [3]. It is clear that a thorough understanding of these soft hadronic final state interactions is required before one can make confident statements regarding QGP production based on charmonium production cross sections [4]. The usefulness of an understanding of these soft processes is now expected to extend well into the deconfined phase, since recent lattice computations indicate that low lying charmonia survive as resonances up to $T \approx 3T_c$ [5].

Unfortunately, little experimental information exists regarding these charmonium dissociation cross sections. Some simple phenomenological estimates based on ‘pre-vector meson dominance’ [6] and absorption cross sections in heavy ion collisions [7] give $\sigma_{tot}^{\psi N} \propto s^{0.22}$ mb and $\sigma_{tot}^{\psi N}(\sqrt{s} \approx 10 \text{ GeV}) \approx 6$ mb respectively. Alternatively, J/ψ photoproduction yields a $J/\psi N$ cross section of approximately 3.5 mb [8] while a combined analysis of J/ψ production from $p + A$ collisions gives a result of 7 mb [9]. For more detailed predictions of the relevant near-threshold cross sections one must employ theoretical models of these scattering processes.

Theoretical estimates have employed a variety of methods, and (perhaps not surprisingly in view of the lack of low-energy experimental data) predict cross sections that vary over several orders of magnitude in the relevant kinematic regime. Early estimates by Kharzeev and Satz [11] using the color-dipole diffractive model of Bhanot and Peskin [10] (which is only justified at high energies) gave extremely small near-threshold $J/\psi N$ total cross sections, typically of microbarn scale. More recently, $J/\psi N$ dissociation cross sections have been estimated using meson exchange models [12, 13], assuming for example t -channel charmed meson exchange or an SU(4)-symmetric hadron effective lagrangian. Results from these models for meson- J/ψ scattering cross sections near thresholds are typically in the few mb range. Similar computations have been reported for $J/\psi N$ scattering [13, 14], which also find total cross sections near threshold in the few mb scale. Although these meson exchange models are of great interest as possibly realistic descriptions of these near-threshold processes they suffer from uncertainties due to poorly understood vertex form factors, Fock space truncations in the set of exchanged particles, and the questionable assumption of higher symmetry groups such as SU(4) (this implicitly assumes a close relationship between the dynamics of pions and heavy-quark $c\bar{c}$ mesons). Regarding hadronic form factors, several groups [16] have found a strong suppression of the predicted dissociation cross sections on incorporating plausible hadronic form factors.

Many of the problems encountered in previous approaches are avoided if one implements a “microscopic” quark-gluon description of these scattering processes, for example using the constituent quark model. The earliest application of this approach to charmonium dissociation is the work of Martin *et al.* [17], who applied the method of Ref. [18] to $J/\psi\pi \rightarrow D^*\bar{D}$ and $D^*\bar{D}^*$ scattering. Martin *et al.* assumed that the confining interaction only operated between $q\bar{q}$ pairs; a more conventional quark-gluon model of charmonium dissociation cross sections based on the usual $\lambda \cdot \lambda$ color structure has been developed by Wong *et al.* [19]. These approaches describe hadronic interactions and bound states in terms of the nonrelativistic quark model, and usually assume that the scattering amplitudes are given to sufficient accuracy at Born order in the quark-gluon interaction (this can be relaxed of course). At Born order in these valence $q\bar{q}$ annihilation free channels hadron-hadron scattering occurs by constituent interchange, and the

scattering amplitudes and cross sections can be derived analytically if sufficiently simple wavefunctions are employed (for example simple harmonic oscillator forms). Applications of this approach to a wide range of similar scattering processes without valence annihilation, such as $I=2 \pi\pi$ [18, 22], KN [20] and NN [21] have shown that this leads to numerically realistic results for many short-ranged S-wave scattering processes.

In this paper we report the first results for charmonium dissociation due to scattering from nucleons in this type of constituent quark scattering model [23]. These amplitudes are also relevant to the time-reversed process of charmonium regeneration, and may prove useful in future studies of bound states of charm and nuclei, as suggested by Brodsky *et al.* [24].

II. QUARK MODEL SCATTERING FORMALISM

The Born-order quark interchange model approximates hadron-hadron scattering as due to a single interaction of the standard quark-model interaction Hamiltonian H_I between all constituent pairs in different hadrons [18]. For the calculations reported here we employ a constituent quark model interaction of the form

$$H_I = \sum_{ij} \left(\frac{\alpha_s}{r_{ij}} - \frac{3}{4} b r_{ij} - \frac{8\alpha_s \sigma^3}{3\sqrt{\pi} m_i m_j} e^{-\sigma^2 r_{ij}^2} S_i \cdot S_j \right) T_i \cdot T_j \quad (1)$$

where the sum extends over all quarks and antiquarks. The three terms in this expression are respectively the color Coulomb interaction, linear confinement, and a regularized contact spin-spin hyperfine interaction. The model parameters have elsewhere been fitted to meson and baryon spectra (see Appendix A for their values).

The color structure of Eq. 1 is given by the usual quadratic perturbative form $T \cdot T$, where $\vec{T} = \vec{\lambda}/2$ for a quark and $-\vec{\lambda}^*/2$ for an antiquark (λ is a Gell-Mann matrix). Meson-baryon systems do not have trivial color dynamics (*i.e.*, a fixed color state with an overall constant color factor), in contrast to mesons and baryons individually, so the assumed color structure of Eq.1 affects the relative amplitudes for different channels. Of course this $T \cdot T$ color structure represents a severe truncation of the full dynamics of the gluonic degrees of freedom. This model does however reproduce the relevant low-energy features of more complete models, and the $T \cdot T$ form is known to be realistic in describing lattice confinement potentials as well as the interactions of low lying hadrons.

We now consider the generic inelastic two-body scattering process $AB \rightarrow CD$, where A is a $c\bar{c}$ charmonium state, B is a nucleon, C is an open-charm ($n\bar{c}$) meson, and D is an open-charm (nnc) baryon. (Here, n is a light u or d quark.) It is convenient to label the quarks as $[\bar{c}c]_{12}[q_1q_2q_3]_{345}$. We choose the (45) quark pair to have definite symmetry under P_{45} quark interchange. Quark interchange scattering in all the systems considered here involves the specific quark permutations P_{23} and $P_{23}P_{34} = P_{34}P_{24}$. By inspection, P_{23} permutations give rise to $D^{-(*)}\Sigma_c^{++}$ final states in $J/\psi(\eta_c)p$ collisions, and $\bar{D}^{0(*)}\Lambda_c^0(\Sigma_c^0)$ states in $J/\psi(\eta_c)n$ collisions. Similarly, $J/\psi(\eta_c)$ interactions involving the permutation operator $P_{23}P_{34}$ give $\bar{D}^{0(*)}\Lambda_c^+(\Sigma_c^+)$ final states, and from $J/\psi(\eta_c)n$ one produces $D^{-(*)}\Lambda_c^+(\Sigma_c^+)$ final states.

Due to P_{45} symmetry only four unique spatial matrix elements are encountered; these are summarized in Table I. The first row gives labels specifying the interaction potentials V_{ij} . Thus for example \bar{d}_1 represents a spatial integral of the form $\int \psi_{13}^* \psi_{245}^* V_{13} \psi_{12} \psi_{345}$.

TABLE I: Spatial Symmetries

perm	13	14	15	23	24	25
P_{23}	\bar{d}_1	\bar{d}_2	\bar{d}_2	d_1	d_2	d_2
$P_{23}P_{34}$	\bar{d}_2	\bar{d}_1	\bar{d}_2	d_2	d_1	d_2

The four unique matrix elements correspond to the four diagrams shown in Fig.1. Note that quark line rearrangement is required to give a nonzero Born-order scattering amplitude, due to the color structure assumed for the quark model interaction. We follow the procedures described in Ref.[18] in evaluating these diagrams. We assume the ‘prior’ form of the scattering amplitude here, in which the separation of the full Hamiltonian into free and interaction parts is specified by the initial hadrons.

Hadronic wavefunctions may generically be written as linear combinations of product basis vectors of the form $\Psi = C\chi\Xi\Phi$, where the individual factors are the color, spin, flavor, and spatial wavefunctions respectively. Explicit wavefunctions for the mesons and baryons considered here are given in Appendix A. Because of this factorizability of the hadron wavefunctions, which involve single factored terms in the cases we consider, the contribution of each quark diagram to the full scattering amplitude can be written as the sum of products of individual color, spin, flavor, and spatial matrix elements.

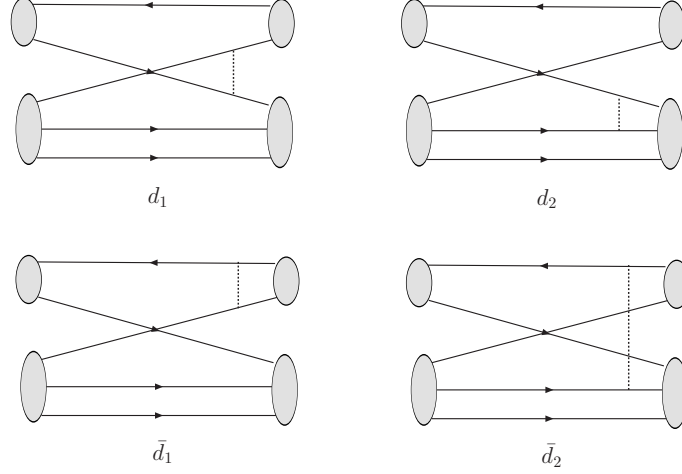


FIG. 1: The four quark-interchange meson-baryon scattering diagrams in the prior formalism.

The Born order scattering amplitudes are then constructed by summing matrix elements of the interaction potential. For the case of P_{23} scattering, for example, we have

$$\mathcal{A} = -\langle P_{23}\Xi_C\Xi_D|\Xi_A\Xi_B\rangle \cdot \sum_{(ij)} \left[\langle P_{23}\mathcal{C}_C\mathcal{C}_D|T_i \cdot T_j|\mathcal{C}_A\mathcal{C}_B\rangle \cdot \langle P_{23}\chi_C\chi_D|S_i \cdot S_j|\chi_A\chi_B\rangle \cdot \langle P_{23}\psi_C\psi_D|V_{ij}|\psi_A\psi_B\rangle \right]. \quad (2)$$

The spin factor $S_i \cdot S_j$ is replaced by unity when considering central (pure potential) interactions. This expression can be simplified using the symmetries and notation discussed above to obtain $\mathcal{A} = -\vec{w} \cdot \vec{d}$, where $\vec{d} = (d_1, d_2, \bar{d}_1, \bar{d}_2)$ and \vec{w} is a weight vector arising from flavor, color, and spin matrix elements. The weight vectors used in this work are listed in Appendix B.

Finally, the charmonium dissociation cross sections were computed from these amplitudes using the expression

$$\sigma = \frac{\mu_{AB}\mu_{CD}}{4\pi^2} \frac{k_f}{k_i} \int |\mathcal{A}|^2 d\Omega \quad (3)$$

where $\mu_{AB} = E_A E_B / (E_A + E_B)$. Charmonium regeneration cross sections can be also obtained using this formalism, since they are related to the dissociation processes by time reversal.

III. CHARMONIUM DISSOCIATION CROSS SECTIONS

A total of 46 exclusive charmonium-nucleon inelastic scattering processes were considered, involving nucleons and the J/ψ or η_c in the initial state and all kinematically accessible open-charm S-wave-meson-baryon channels in the final state. Specifically, we have computed total cross sections for the following reactions:

$$J/\psi p; \eta_c p \rightarrow \bar{D}^0 \Lambda_c^+; \bar{D}^0 \Sigma_c^+; \bar{D}^{0*} \Lambda_c^+; \bar{D}^{0*} \Sigma_c^+; D^- \Sigma_c^{++}; D^{*-} \Sigma_c^{++} \quad (4)$$

$$J/\psi n; \eta_c n \rightarrow \bar{D}^0 \Sigma_c^0; \bar{D}^{0*} \Sigma_c^0; D^- \Sigma_c^+; D^{*-} \Sigma_c^+; D^- \Lambda_c^+; D^{*-} \Lambda_c^+ \quad (5)$$

$$[J/\psi p]_{3/2} \rightarrow \bar{D}^{0*} \Sigma_{c3/2}^+; D^{*-} \Sigma_{c3/2}^{++}; \bar{D}^0 \Sigma_{c3/2}^+; D^- \Sigma_{c3/2}^{++} \quad (6)$$

$$[J/\psi n]_{3/2} \rightarrow \bar{D}^{0*}\Sigma_{c3/2}^0; D^{-*}\Sigma_{c3/2}^+; \bar{D}^0\Sigma_{c3/2}^0; D^-\Sigma_{c3/2}^+ \quad (7)$$

$$[J/\psi p]_{1/2}; \eta_c p \rightarrow \bar{D}^{0*}\Sigma_{c3/2}^+; D^{-*}\Sigma_{c3/2}^{++} \quad (8)$$

and

$$[J/\psi n]_{1/2}; \eta_c n \rightarrow \bar{D}^{0*}\Sigma_{c3/2}^0; D^{-*}\Sigma_{c3/2}^+. \quad (9)$$

Isospin symmetry and the equivalence of many quark line diagrams imply that all the $J/\psi(\eta_c)n$ amplitudes are simply related to $J/\psi(\eta_c)p$ amplitudes, as follows:

$$\mathcal{A}(J/\psi(\eta_c)n \rightarrow \bar{D}^{0(*)}\Sigma_c^0) = \mathcal{A}(J/\psi(\eta_c)p \rightarrow D^{-(*)}\Sigma_c^{++}) \quad (10)$$

and

$$\mathcal{A}(J/\psi(\eta_c)n \rightarrow D^{-(*)}\Sigma_c^+(\Lambda_c^+)) = \mathcal{A}(J/\psi(\eta_c)p \rightarrow \bar{D}^{0(*)}\Sigma_c^+(\Lambda_c^+)). \quad (11)$$

Thus 23 unique amplitudes remain to be computed.

An additional isospin relation between these reactions can be derived because the $D^-\Sigma_c^{++}$ and $\bar{D}^0\Sigma_c^+$ states both couple to $|II_z\rangle = |\frac{1}{2}\frac{1}{2}\rangle$. Thus

$$\frac{\mathcal{A}(J/\psi p \rightarrow \bar{D}^0\Sigma_c^+)}{\mathcal{A}(J/\psi p \rightarrow D^-\Sigma_c^{++})} = -\frac{1}{\sqrt{2}}. \quad (12)$$

This relationship evidently holds for the weights reported in Appendix B, which were derived without making this assumption.

The cross sections we find using this approach typically rise rapidly at threshold, and then are strongly damped above a hadron momentum scale set by the hadronic wavefunctions. Since the hyperfine, Coulomb, and linear confinement contributions vary in sign within channels and have very different momentum dependences, secondary peaks can appear (see Figs.2,3), although these tend to be much weaker than the near-threshold maxima. In three instances this pattern is reversed; one of these is shown in the right panel of Fig.2.

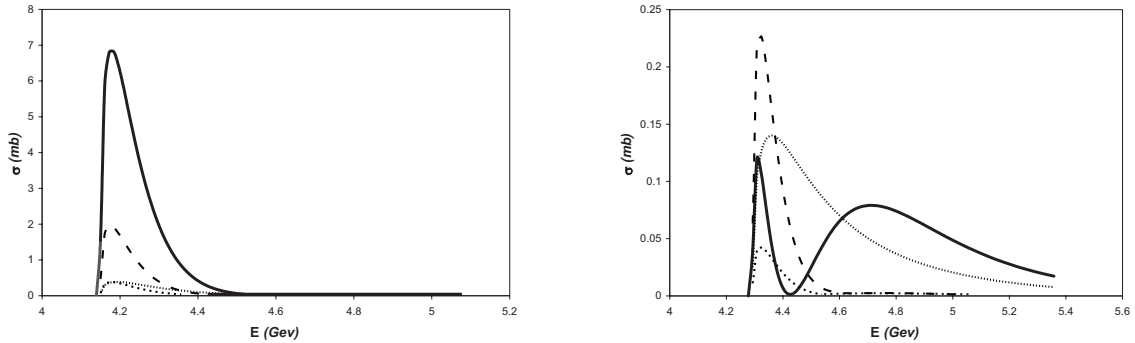


FIG. 2: $J/\psi p \rightarrow \bar{D}^0\Lambda_c^+$ (left) $J/\psi p \rightarrow \bar{D}^{0*}\Lambda_c^+$ (right). Curves are: total cross section (solid), hyperfine (dotted), linear (dashed), Coulomb (small dash).

We summarize all 23 independent cross sections in Tables II-IV. The columns in these tables specify the energies and values of the near-threshold maxima (point 1), the subsequent minimum (point 2), and the secondary maximum (point 3), if it is significant.

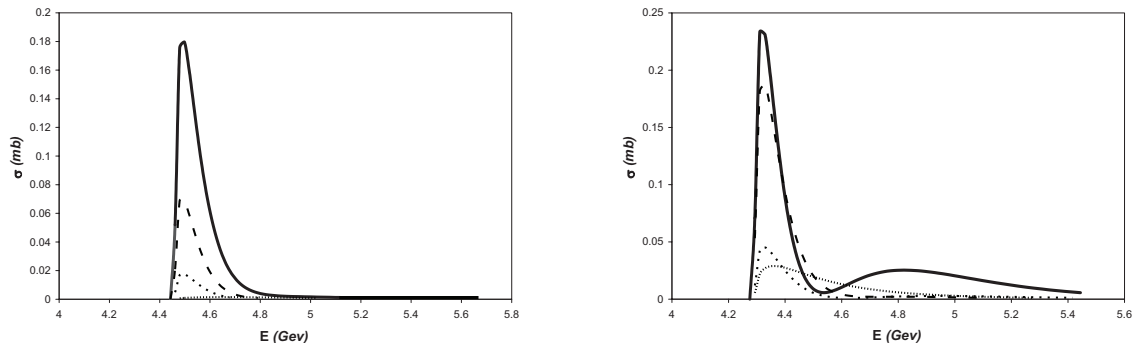


FIG. 3: $J/\psi p \rightarrow \bar{D}^{0*}\Sigma_c^+$ (left) $\eta_c p \rightarrow D^-\Sigma_c^{++}$ (right). Curves are: total cross section (solid), hyperfine (dotted), linear (dashed), Coulomb (small dash).

TABLE II: $\eta_c p$ Cross Sections.

Final State	$(E(\text{GeV}), \sigma(\text{mb}))_1$	$(E(\text{GeV}), \sigma(\text{mb}))_2$	$(E(\text{GeV}), \sigma(\text{mb}))_3$
$\bar{D}^0\Lambda_c^+$	(4.196 , 1.190)		
$\bar{D}^0\Sigma_c^+$	(4.355 , 0.221)		
$D^-\Sigma_c^{++}$	(4.360 , 0.432)		
$\bar{D}^{0*}\Lambda_c^+$	(4.311 , 0.233)	(4.527 , 0.006)	(4.820 , 0.025)
$\bar{D}^{0*}\Sigma_c^+$	(4.5021 , 0.0073)	(4.8162 , 0.0001)	(5.1164 , 0.0003)
$\bar{D}^{0*}\Sigma_c^{3/2}$	(4.547 , 0.018)	(4.702 , 0.003)	(4.966 , 0.008)
$D^{*-}\Sigma_c^{++}$	(4.5050 , 0.0144)	(4.8195 , 0.0001)	(5.1199 , 0.0005)
$D^{*-}\Sigma_c^{3/2}$	(4.551 , 0.009)	(4.706 , 0.001)	(4.971 , 0.004)

IV. DISCUSSION AND CONCLUSIONS

The most important process is $J/\psi p \rightarrow \bar{D}^0\Lambda_c^+$ scattering, with a peak cross section of approximately 7 mb (Fig. 2). Next in strength is $J/\psi p \rightarrow D^{0*}\Lambda_c^+$, with a maximum near 1.7 mb. These results disagree with meson exchange models, for example Liu, Ko, and Lin[14] find a larger cross section for $D^*\Lambda_c$ scattering than $D\Lambda_c$ while Sibirtsev, Tsushima, and Thomas[14] find roughly comparable cross sections.

The total dissociation cross section is shown in Fig. 4. It is clear that the quark model description of charm dissociation is not in agreement with the widely held view that the absorption cross section should be constant. In general cross sections increase with phase space and then are strongly damped due to the finite size of hadronic wavefunctions. Although this effect can be overcome by the opening of many channels, it is evident that this does not occur up to center of mass energies of 5 GeV or more. This observation is in disagreement with typical meson exchange models, which tend to find slowly increasing total cross sections. Presumably this behaviour is due to (approximately) cancelling momentum dependence between vertices with derivative coupling and monopole form factors. While the momentum dependence of quark model vertices must agree with their hadronic analogues (see, for example, Ref. [25]), quark model form factors fall much more rapidly in momentum than the power law monopole form factors, providing a possible source of the discrepancy.

We remark that the quark exchange computation presented here can be regarded as the short range component of J/ψ dissociation in scattering from nucleons. Long range dissociation can occur via virtual pion emission from the nucleon giving rise to reactions such as $J/\psi N \rightarrow \bar{D}D^*N$. This amplitude can be related to that of $J/\psi\pi \rightarrow \bar{D}D^*$ scattering, which is relevant to comover absorption. This has been done, for example, by Liu, Ko, and Lin[14] who obtain asymptotic cross sections of order 1 mb for each of $J/\psi N \rightarrow \bar{D}D^*N$, \bar{D}^*DN , and $\bar{D}DN$. Of course, their results depend on theoretical $J/\psi\pi$ scattering cross sections as computed in the meson exchange formalism. Unfortunately, these are strongly dependent on form factors; for example $J/\psi\pi \rightarrow \bar{D}D^*$ ranges from 20 mb at large \sqrt{s} with no form factor to 4 mb with a form factor cutoff of 1 GeV. Alternatively, quark model computations of the same reaction give maximum cross sections of order 1/2 mb just above threshold[19], in keeping with phenomenological estimates of comover absorption[7, 26]. From these considerations we conclude that the long range contribution to charmonium dissociation by nucleons is small (less than 1 mb).

Comparison with experiment is difficult at present. As mentioned in the Introduction, J/ψ photoproduction and $p+A$ collisions yield estimates of 3.5 mb and 7 mb respectively. However these estimates are made assuming constant cross sections, and it appears unlikely that this is accurate. Nevertheless, the average near-threshold strength of our

TABLE III: $J/\psi p$ ($S = 1/2$) Cross Sections.

Final State	$(E(\text{GeV}), \sigma(\text{mb}))_1$	$(E(\text{GeV}), \sigma(\text{mb}))_2$	$(E(\text{GeV}), \sigma(\text{mb}))_3$
$\bar{D}^0 \Lambda_c^+$	(4.184 , 6.815)	(4.619 , 0.010)	(4.884 , 0.022)
$\bar{D}^0 \Sigma_c^+$	(4.350 , 0.126)		
$D^- \Sigma_c^{++}$	(4.355 , 0.246)		
$\bar{D}^{0*} \Lambda_c^+$	(4.308 , 0.120)	(4.425 , 0.001)	(4.703 , 0.079)
$\bar{D}^{0*} \Sigma_c^+$	(4.498 , 0.180)		
$\bar{D}^{0*} \Sigma_{c3/2}^+$	(4.545 , 0.009)	(4.668 , 0.002)	(4.891 , 0.005)
$D^{*-} \Sigma_c^{++}$	(4.501 , 0.354)		
$D^{*-} \Sigma_{c3/2}^+$	(4.549 , 0.017)	(4.672 , 0.004)	(4.896 , 0.009)

TABLE IV: $J/\psi p$ ($S = 3/2$) Cross Sections.

Final State	$(E(\text{GeV}), \sigma(\text{mb}))_1$	$(E(\text{GeV}), \sigma(\text{mb}))_2$	$(E(\text{GeV}), \sigma(\text{mb}))_3$
$\bar{D}^0 \Sigma_{c3/2}^+$	(4.418 , 0.276)	(4.873 , 0.000)	(5.165 , 0.001)
$D^- \Sigma_{c3/2}^{++}$	(4.424 , 0.536)	(4.881 , 0.001)	(5.173 , 0.002)
$\bar{D}^{0*} \Lambda_c^+$	(4.324 , 1.712)	(4.639 , 0.021)	(4.791 , 0.027)
$\bar{D}^{0*} \Sigma_c^+$	(4.498 , 0.054)		
$\bar{D}^{0*} \Sigma_{c3/2}^+$	(4.545 , 0.042)	(4.733 , 0.002)	(4.986 , 0.006)
$D^{*-} \Sigma_c^{++}$	(4.501 , 0.106)		
$D^{*-} \Sigma_{c3/2}^+$	(4.549 , 0.082)	(4.737 , 0.004)	(4.991 , 0.012)

total cross section seems in accord with these phenomenological estimates.

Finally, the strong near-threshold behaviour seen here implies that it would be worthwhile to revisit hydrodynamic simulations of charmonium suppression in heavy ion collisions. In this regard, we note that the current computation deals with free charmonium scattering, rather than the “pre”-charmonium expected in RHIC collisions. Furthermore, substantial density dependence may be present[27] and this should be taken into account when applying these predictions to a nuclear environment.

Acknowledgments

We are grateful to Che-Ming Ko and Berndt Mueller for communications on this research. This work was supported by the U.S. Department of Energy under contract DE-FG02-00ER41135 and the U.S. National Science Foundation under grant NSF-PHY-244668 at the University of Pittsburgh, the U.S. National Science Foundation through grant NSF-PHY-0244786 at the University of Tennessee, and the U.S. Department of Energy under contract DE-AC05-00OR22725 at Oak Ridge National Laboratory.

-
- [1] T. Matsui and H. Satz, Phys. Lett. B **178**, 416 (1986).
 - [2] R. Vogt, Phys. Rept. **310**, 197 (1999).
 - [3] P. Braun-Munzinger and J. Stachel, Phys. Lett. B **490**, 196 (2000) [arXiv:nucl-th/0007059]; R. L. Thews, M. Schroedter and J. Rafelski, Phys. Rev. C **63**, 054905 (2001) [arXiv:hep-ph/0007323].
 - [4] The status of theoretical computations is reviewed in T. Barnes, arXiv:nucl-th/0306031. (Proceedings of QNP-2002, Jülich, Germany, 9-14 Jun 2002.)
 - [5] S. Datta, F. Karsch, P. Petreczky and I. Wetzorke, Phys. Rev. D **69**, 094507 (2004) [arXiv:hep-lat/0312037]. T. Umeda, K. Nomura and H. Matsufuru, Eur. Phys. J. C **39S1**, 9 (2005) [arXiv:hep-lat/0211003].
 - [6] J. Hüfner and B. Kopeliovich, Phys. Lett. B **426**, 154 (1998).
 - [7] G. Gerschel, J. Hüfner and E. Quack, J. Phys. G **22**, 1335 (1996) [arXiv:hep-ph/9502299]. See also A. Capella, A. Kaidalov, A. Kouider Akil and C. Gerschel, Phys. Lett. B **393**, 431 (1997) [arXiv:hep-ph/9607265].
 - [8] R.L. Anderson *et al.*, Phys. Rev. Lett. **38**, 263 (1977).
 - [9] D. Kharzeev, C. Lourenço, M. Nardi and H. Satz, Z. Phys. C **74**, 307 (1997) [arXiv:hep-ph/9612217].
 - [10] G. Bhanot and M. E. Peskin, Nucl. Phys. B **156**, 391 (1979).
 - [11] D. Kharzeev and H. Satz, Phys. Lett. B **334**, 155 (1994) [arXiv:hep-ph/9405414]. For more recent work see F. Arleo, P. B. Gossiaux, T. Gousset and J. Aichelin, Phys. Rev. D **65**, 014005 (2002) [arXiv:hep-ph/0102095]; Y. Oh, S. Kim and S. H. Lee, Phys. Rev. C **65**, 067901 (2002) [arXiv:hep-ph/0111132].

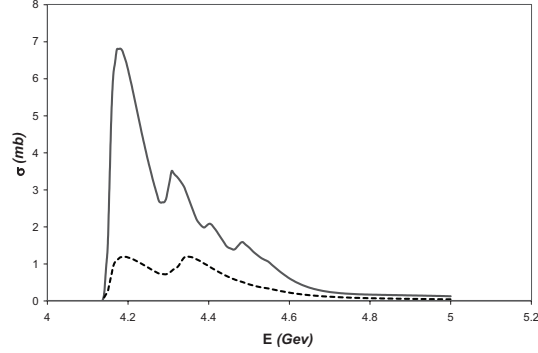


FIG. 4: Total Charmonium Dissociation Cross Sections. $J/\psi N$ (solid); $\eta_c N$ (dashed).

- [12] S. G. Matinian and B. Müller, Phys. Rev. C **58**, 2994 (1998) [arXiv:nucl-th/9806027]; K. L. Haglin and C. Gale, Phys. Rev. C **63**, 065201 (2001) [arXiv:nucl-th/0010017]; A. Bourque, C. Gale and K. L. Haglin, Phys. Rev. C **70**, 055203 (2004) [arXiv:hep-ph/0408048].
- [13] K. L. Haglin, Phys. Rev. C **61**, 031902 (2000) [arXiv:nucl-th/9907034].
- [14] A. Sibirtsev, K. Tsushima and A. W. Thomas, Phys. Rev. C **63**, 044906 (2001) [arXiv:nucl-th/0005041]; W. Liu, C. M. Ko and Z. W. Lin, Phys. Rev. C **65**, 015203 (2002) [arXiv:nucl-th/0107058].
- [15] A. Sibirtsev and M. B. Voloshin, Phys. Rev. D **71**, 076005 (2005) [arXiv:hep-ph/0502068].
- [16] Z. W. Lin and C. M. Ko, Phys. Rev. C **62**, 034903 (2000) [arXiv:nucl-th/9912046]; Y. Oh, T. Song and S. H. Lee, Phys. Rev. C **63**, 034901 (2001) [arXiv:nucl-th/0010064]; Y. S. Oh, T. S. Song, S. H. Lee and C. Y. Wong, J. Korean Phys. Soc. **43**, 1003 (2003) [arXiv:nucl-th/0205065].
- [17] K. Martins, D. Blaschke and E. Quack, Phys. Rev. C **51**, 2723 (1995) [arXiv:hep-ph/9411302].
- [18] T. Barnes and E. S. Swanson, Phys. Rev. D **46**, 131 (1992); E. S. Swanson, Annals Phys. **220**, 73 (1992).
- [19] C. Y. Wong, E. S. Swanson and T. Barnes, Phys. Rev. C **65**, 014903 (2002) [Erratum-ibid. C **66**, 029901 (2002)]; C. Y. Wong, E. S. Swanson and T. Barnes, Phys. Rev. C **62**, 045201 (2000).
- [20] T. Barnes and E. S. Swanson, Phys. Rev. C **49**, 1166 (1994).
- [21] T. Barnes, S. Capstick, M. D. Kovarik and E. S. Swanson, Phys. Rev. C **48**, 539 (1993) [arXiv:nucl-th/9302007].
- [22] T. Barnes, E. S. Swanson and J. D. Weinstein, Phys. Rev. D **46**, 4868 (1992) [arXiv:hep-ph/9207251].
- [23] A previous computation has been made with a quark-diquark model of the nucleon: K. Martins, Prog. Part. Nucl. Phys. **36**, 409 (1996) [arXiv:hep-ph/9601314].
- [24] S. J. Brodsky, I. A. Schmidt and G. F. de Teramond, Phys. Rev. Lett. **64**, 1011 (1990).
- [25] C. Downum, T. Barnes, J. R. Stone and E. S. Swanson, Phys. Lett. B **638**, 455 (2006) [arXiv:nucl-th/0603020].
- [26] A. Capella, E. G. Ferreira and A. B. Kaidalov, Phys. Rev. Lett. **85**, 2080 (2000) [arXiv:hep-ph/0002300].
- [27] A. Sibirtsev, K. Tsushima, K. Saito and A. W. Thomas, Phys. Lett. B **484**, 23 (2000) [arXiv:nucl-th/9904015].

APPENDIX A: HADRONIC WAVEFUNCTIONS

Total baryon wavefunctions were constructed as follows:

$$N = \mathcal{C}\Xi_N\Phi_B\chi^\lambda, \quad (\text{A1})$$

$$\Lambda_c = \mathcal{C}\Xi_\Lambda\Phi_D\chi^\rho, \quad (\text{A2})$$

$$\Sigma_c = \mathcal{C}\Xi_\Sigma\Phi_D\chi^\lambda, \quad (\text{A3})$$

$$\Sigma_{c3/2} = \mathcal{C}\Xi_\Sigma\Phi_D\chi^{3/2} \quad (\text{A4})$$

where

$$\Xi_{\Lambda} = \frac{1}{\sqrt{2}}c(ud - du), \quad (\text{A5})$$

$$\Xi_{\Sigma^{++}} = cuu, \quad (\text{A6})$$

$$\Xi_{\Sigma^+} = \frac{1}{\sqrt{2}}c(ud + du), \quad (\text{A7})$$

$$\Xi_{\Sigma^0} = cdd. \quad (\text{A8})$$

The baryon color wavefunction is given by

$$\mathcal{C} = \frac{1}{\sqrt{6}}\epsilon_{abc} \quad (\text{A9})$$

where ϵ is the rank three antisymmetric Cartesian tensor in color indices.

Baryon spin wavefunctions are (only top states are given)

$$\chi_{\frac{1}{2}\frac{1}{2}}^{\lambda} = -\frac{1}{\sqrt{6}}(|++-\rangle + |+-+\rangle - 2| - ++\rangle), \quad (\text{A10})$$

$$\chi_{\frac{1}{2}\frac{1}{2}}^{\rho} = \frac{1}{\sqrt{2}}(|++-\rangle - |+-+\rangle), \quad (\text{A11})$$

and

$$\chi_{\frac{3}{2}\frac{3}{2}}^{3/2} = |+++ \rangle. \quad (\text{A12})$$

The spatial wavefunctions are

$$\Phi_A = \frac{1}{\beta_A^{3/2}\pi^{3/4}} \exp\left(-\frac{p_{rel}^2}{2\beta_A^2}\right) \quad (\text{A13})$$

$$\Phi_B = \frac{3^{3/4}}{\pi^{3/2}\alpha^3} \exp\left(-\frac{p_{\rho}^2 + p_{\lambda}^2}{2\alpha_{\rho}^2}\right) \quad (\text{A14})$$

$$\Phi_C = \frac{1}{\beta_C^{3/2}\pi^{3/4}} \exp\left(-\frac{p_{rel}^2}{2\beta_C^2}\right) \quad (\text{A15})$$

$$\Phi_D = \frac{3^{3/4}}{\pi^{3/2}\alpha_{\rho}^{3/2}\alpha_{\lambda}^{3/2}} \exp\left(-\frac{p_{\rho}^2}{2\alpha_{\rho}^2} - \frac{p_{\lambda}^2}{2\alpha_{\lambda}^2}\right) \quad (\text{A16})$$

with

$$p_{rel} = \frac{m_2 p_1 - m_1 p_2}{m_1 + m_2}, \quad (\text{A17})$$

$$p_{\rho} = \sqrt{\frac{1}{2}} \frac{(m_3 + 2m_5)p_4 - (m_3 + 2m_4)p_5 + (m_5 - m_4)p_3}{m_4 + m_5 + m_3}, \quad (\text{A18})$$

$$p_{\lambda} = \sqrt{\frac{3}{2}} \frac{m_3(p_4 + p_5) - (m_4 + m_5)p_3}{m_4 + m_5 + m_3}. \quad (\text{A19})$$

SHO meson and baryon wavefunctions can be expected to be reasonably accurate for hadrons composed of light quarks or heavy-light mesons. However, they are not reliable for Coulombic systems such as charmonium. Thus in our computations the nominal charmonium wavefunction (Φ_A above) has been replaced with a sum over Gaussians that accurately replicates the numerically obtained wavefunction. The subsequent change in the cross section is illustrated in Fig. 5, where the importance of an accurate charmonium wavefunction near scattering threshold is evident.

All model parameters have been fixed by meson and baryon spectroscopy. The parameters used here are listed in Table V.

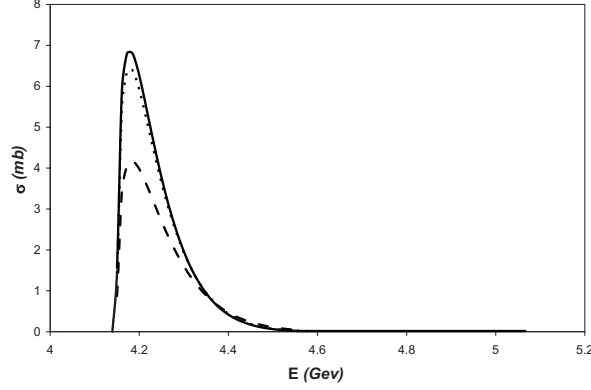


FIG. 5: $\sigma(\psi p \rightarrow \bar{D}^0 \Lambda_c)$. Single J/ψ SHO (dashed), six Gaussians (dotted), ten Gaussians (solid).

TABLE V: Model Parameters. All units are GeV except b (GeV^2) and α_s .

m_u	m_c	b	α_s	β_ψ	β_η	β_D	β_{D^*}	α_N	α_ρ	α_λ
0.33	1.5	0.162	0.594	0.67	0.74	0.44	0.38	0.3	0.3	0.45

Note that in an SHO (Isgur-Karl) model one has the relationships

$$\alpha_\rho = (3km)^{1/4}$$

and

$$\alpha_\lambda = (3km_\lambda)^{1/4}$$

with

$$m_\lambda = \frac{3mM}{2m + M}$$

where M is the mass of quark 3.

APPENDIX B: WEIGHTS

The color matrix elements required in the evaluation of the scattering amplitudes we evaluate are listed in Table VI below.

TABLE VI: Color Matrix Elements

perm	13	14	15	23	24	25
P_{23}	$-\frac{4}{9}$	$\frac{2}{9}$	$\frac{2}{9}$	$\frac{4}{9}$	$-\frac{2}{9}$	$-\frac{2}{9}$
$P_{23}P_{34}$	$-\frac{2}{9}$	$\frac{4}{9}$	$-\frac{2}{9}$	$\frac{2}{9}$	$-\frac{4}{9}$	$\frac{2}{9}$

With the spatial symmetries specified in Sect. II, weights are computed as follows

$$w_1 = \langle P_{23} \Xi_C \Xi_D | \Xi_A \Xi_B \rangle \langle P_{23} \chi_C \chi_D | \chi_A \chi_B \rangle \langle P_{23} \mathcal{C}_C \mathcal{C}_D | T_2 \cdot T_3 | \mathcal{C}_A \mathcal{C}_B \rangle \quad (\text{B1})$$

and

$$w_2 = \langle P_{23} \Xi_C \Xi_D | \Xi_A \Xi_B \rangle \langle P_{23} \chi_C \chi_D | \chi_A \chi_B \rangle \langle P_{23} \mathcal{C}_C \mathcal{C}_D | T_2 \cdot T_4 + T_2 \cdot T_5 | \mathcal{C}_A \mathcal{C}_B \rangle. \quad (\text{B2})$$

Similar expressions hold for w_3 and w_4 . Here we consider the case of P_{23} scattering through a central potential. Substituting the color matrix elements of Table VI then yields

$$\vec{w} = \frac{4}{9} \langle P_{23} \Xi_C \Xi_D | \Xi_A \Xi_B \rangle \langle P_{23} \chi_C \chi_D | \chi_A \chi_B \rangle (1, -1, -1, 1). \quad (\text{B3})$$

The prefactor in this expression is reported in the column labelled ‘Coulomb and linear’ in the tables below. The spin-dependence of the hyperfine interaction does not permit simplification, hence the entire weight vectors are specified.

TABLE VII: $J/\psi p$, $S = 1/2$ Weights.

Final State	hyperfine	Coulomb and linear
$\bar{D}^0 \Lambda_c^+$	$\frac{\sqrt{2}}{12} [-1, 0, 3, 0]$	$\frac{\sqrt{2}}{3}$
$\bar{D}^0 \Sigma_c^+$	$\frac{\sqrt{6}}{108} [1, -2, -3, -2]$	$-\frac{\sqrt{6}}{27}$
$\bar{D}^{0*} \Lambda_c^+$	$\frac{\sqrt{6}}{36} [5, 0, 1, 0]$	$-\frac{\sqrt{6}}{9}$
$\bar{D}^{0*} \Sigma_c^+$	$\frac{\sqrt{2}}{108} [7, 10, -5, -6]$	$\frac{5\sqrt{2}}{27}$
$D^- \Sigma_c^{++}$	$\frac{\sqrt{3}}{54} [-1, 2, 3, 2]$	$\frac{2\sqrt{3}}{27}$
$D^{-*} \Sigma_c^{++}$	$\frac{1}{54} [-7, -10, 5, 6]$	$-\frac{10}{27}$
$\bar{D}^{0*} \Sigma_{c3/2}^+$	$\frac{1}{27} [1, 1, 1, 3]$	$\frac{4}{27}$
$D^{-*} \Sigma_{c3/2}^{++}$	$-\frac{\sqrt{2}}{27} [1, 1, 1, 3]$	$\frac{4\sqrt{2}}{27}$

TABLE VIII: $J/\psi p$, $S = 3/2$ Weights.

Final State	hyperfine	Coulomb and linear
$\bar{D}^{0*} \Lambda_c^+$	$\frac{\sqrt{6}}{18} [1, 0, -1, 0]$	$\frac{2\sqrt{6}}{9}$
$\bar{D}^{0*} \Sigma_c^+$	$\frac{\sqrt{2}}{54} [5, 2, -1, 0]$	$\frac{2\sqrt{2}}{27}$
$D^{-*} \Sigma_c^{++}$	$-\frac{1}{27} [5, 2, -1, 0]$	$-\frac{4}{27}$
$\bar{D}^{0*} \Sigma_{c3/2}^+$	$-\frac{\sqrt{10}}{54} [1, 1, 1, 0]$	$\frac{2\sqrt{10}}{27}$
$D^{-*} \Sigma_{c3/2}^{++}$	$-\frac{\sqrt{5}}{27} [1, 1, 1, 0]$	$-\frac{4\sqrt{5}}{27}$
$\bar{D}^0 \Sigma_{c3/2}^+$	$-\frac{\sqrt{6}}{54} [1, 1, -3, -2]$	$\frac{2\sqrt{6}}{27}$
$D^- \Sigma_{c3/2}^{++}$	$\frac{\sqrt{3}}{27} [1, 1, -3, -2]$	$-\frac{4\sqrt{3}}{27}$

TABLE IX: $\eta_c p$ Weights.

Final State	hyperfine	Coulomb and linear
$\bar{D}^0 \Lambda_c^+$	$\frac{\sqrt{6}}{12} [1, 0, 1, 0]$	$\frac{\sqrt{6}}{9}$
$\bar{D}^0 \Sigma_c^+$	$\frac{\sqrt{2}}{36} [3, 2, 3, 2]$	$\frac{\sqrt{2}}{9}$
$\bar{D}^{0*} \Lambda_c^+$	$-\frac{\sqrt{2}}{12} [1, 0, 1, 0]$	$\frac{\sqrt{2}}{3}$
$\bar{D}^{0*} \Sigma_c^+$	$\frac{\sqrt{6}}{108} [1, -2, 1, -2]$	$-\frac{\sqrt{6}}{27}$
$D^- \Sigma_c^{++}$	$-\frac{1}{18} [3, 2, 3, 2]$	$-\frac{2}{9}$
$D^{-*} \Sigma_c^{++}$	$-\frac{\sqrt{3}}{54} [1, -2, 1, -2]$	$\frac{2\sqrt{3}}{27}$
$\bar{D}^{0*} \Sigma_{c3/2}^+$	$\frac{\sqrt{12}}{54} [1, 1, 1, 1]$	$-\frac{2\sqrt{12}}{27}$
$D^{-*} \Sigma_{c3/2}^{++}$	$-\frac{\sqrt{6}}{27} [1, 1, 1, 1]$	$\frac{4\sqrt{6}}{27}$